

Geometry dependence on the energy of topological vortices on surfaces with negative and variable curvature

Vagson L. Carvalho-Santos*

*Instituto Federal de Educação, Ciência e Tecnologia Baiano - Campus Senhor do Bonfim
48970-000 Senhor do Bonfim, Bahia, Brazil*

Felipe A. Apolonio

*Departamento de Física, Universidade Federal de Viçosa
36570-000 Viçosa, Minas Gerais, Brazil*

Abstract

We have applied the Anisotropic Heisenberg Model on the surfaces of the catenoid and hyperboloid, which present negative and variable curvature. Two kinds of topological excitations were considered. The first one is given when we take $\lambda = 0$ (isotropic model), which leads to the sine-Gordon equation and a π -soliton-like solution is obtained. This corresponds to the first class of the second homotopy group of the spin sphere mapping. The second one is given by $\lambda = -1$, that consists of the XY model, whose solution can be a vortex turning around the surfaces. The results show that the vortex energy depends of the length scale of the underlying geometry and, for small central radius (CR), the hyperboloid presents lower vortex energy than that on a catenoid, which, as well as the cylinder case, has its vortex energy varying with the characteristic length $1/\rho$. We have also shown that for any CR value, the lowest value of the vortex energy occurs on the polar hyperboloid surface.

I. INTRODUCTION

Geometrical and topological concepts and tools are important in many branches of natural sciences, particularly, in Physics. For instance, the idea of symmetry, which is intimately associated with geometry, is a keystone for studying a number of fundamental properties of several physical systems, e.g., the Noether theorem asserts that there is a conserved quantity to each continuous symmetry of the associated action. Topology, in turn, is crucial for classifying and for giving stability to certain excitations, such as solitons, extending objects having finite energy, and vortices, presenting a nonvanishing vorticity around a given singular point or a topological obstruction. In addition, the observed vortex-pair dissociation is the mechanism behind the topological phase transition¹.

Vortices and solitons are particle-like excitations and their behavior in different geometries has remained largely unexplored experimentally and is of growing theoretical interest². These and others have been observed in a number of systems, such as superconductors, superfluids, and magnetic materials^{3,4}. In nanomagnets, depending on the length and thickness of micro-sized disks, a vortex can appear in their centers⁵ and the dynamic behavior of the vortices is affected by structural defects that appear during the nanoparticles fabrication. For instance, it is observed that the interaction of the out-of-plane component of vortices with curved defects in nanomagnets must cause a chiral symmetry breaking in the vortex gyrotropic motion due to the thin-film roughness⁶ and still, in-plane vortices on a two-dimensional space interact not only with each other, but also with the curvature of the substrate⁷. Besides, the energy of these excitations, as well as their stability, depends on the shape of the nanoparticle⁸. In this context, small curved hills and valleys in magnetic nanodots can be modeled by point-like defects, the mathematical representation of which can be given by the Dirac delta function⁹.

On the other hand, vortices can appear like solutions of the two-dimensional continuous Heisenberg Model and have been considered in many curved geometries, as the torus^{10,11}, pseudosphere¹², sphere¹³, cylinder¹⁴ and cone¹⁵. In these works, the authors analyse the dynamic and static properties of vortices and solitons. The results show that the vortex energy is closely linked to the characteristic length of the considered geometry and still, for holeless surfaces, this energy presents a divergence, which can be controlled by the development of an out-of-plane component in the vortex core, so called the vortex polarity. Soliton-like so-

lution also have been considered in those works and it is shown that its characteristic length depends on the length scale of the surface and, for finite surfaces, half-soliton solutions are found^{12,16}. Kravchuk *et al* showed that the easy-surface Heisenberg model in spherical shells leads to a coupling between the localized out-of-surface component of the vortex with its delocalized in-surface structure¹⁷, what is associated with the curvature of the underlying surface.

From the viewpoint of fundamental physics, the curvature of a surface can induce a quantum potential in the Schrödinger equation, which alters the form of the groundstate and excited-state wavefunctions¹⁸. Thus, an important task would be to control the shape of membranes, what can be done, for example, by the knowledge of their magnetic properties. This way, Saxena *et al.* have considered the exchange and Zeeman terms in the magnetic energy calculations for cylindrical surfaces, and showed that the interaction of an external magnetic field with a cylindrical magnetoelastic membrane has a 2π soliton-like solution, what induces a deformation (pinch) at the point where the spins are pointing in the opposite direction to the magnetic field¹⁹.

In this paper, we propose the study of the anisotropic Heisenberg Model on the catenoid and hyperboloid, which are surfaces with variable and negative curvature and present cylindrical symmetry. To our knowledge, the isotropic Heisenberg Model was previously applied on the surfaces of the catenoid, helicoid, the single-sheet paraboloid and hyperboloid²² and the authors obtained skyrmion-like solutions. Here, we extended their analysis by studying both soliton-like ($\lambda = 0$ case) and vortex-like ($\lambda = -1$ case) solutions. Our main objective is to study a class of topological excitations on these surfaces, as well as the influence of a characteristic length, associated with each geometry, on the vortex energy. The answers for these questions may be relevant for future researches in nanomagnetism, once they can improve the understanding of curvature effects in the static and dynamic behavior of vortices in ferromagnetic curved nanoparticles. In fact, the possibility of miniaturization of magnetic devices is an attractive proposition, since circular nanomagnets with vortex as the magnetization groundstate have been considered as candidates in the composition of data storage devices²⁰ and nanoparticles for cancer therapy²¹.

We have observed that, for small central radius (CR), the energy of a vortex on a hyperboloid is lower than that on a catenoid, however unlike what was observed on other geometries (cylinder, torus and catenoid, for example), the vortex energy on the hyper-

boloid surface does not vanish when CR tends to infinity. Indeed, we have shown that the vortex energy tends asymptotically to $2\pi \ln(1+h^2)$, where h is the height of the hyperboloid. Furthermore, the polar hyperboloid presents the lowest energy when compared with the catenoid and the cylinder. This fact can, at first sight, indicate that circular nanomagnets with polar hyperboloid shape could sustain a vortex as the magnetization groundstate to smaller radius than those appearing in magnetic nanorings. However, to confirm this hypothesis, the magnetostatic and exchange energies must be taken into account for different magnetization configurations and the volume of the nanomagnet must be considered.

To proceed our analysis, this work is organized as follows: in Section II we present the continuous anisotropic Heisenberg Model, in Section III, we apply this model to the surfaces of the catenoid and hyperboloid. The Section IV brings the results and discussions, and compare our results with that obtained for the surface of a cylinder. Finally, in the Section V, we present our conclusions and prospects for future works.

II. CONTINUUM HEISENBERG MODEL

The anisotropic exchange Heisenberg model, for nearest neighbor interacting spins on a two-dimensional lattice, is given by the Hamiltonian below:

$$H_{\text{latt}} = -J' \sum_{\langle i,j \rangle} [m_i^x m_j^x + m_i^y m_j^y + (1 + \lambda) m_i^z m_j^z], \quad (1)$$

where J' denotes the coupling between neighboring spins, and according to $J' < 0$ or $J' > 0$, the Hamiltonian describes a ferro or antiferromagnetic system, respectively. $\vec{m}_i = (m_i^x, m_i^y, m_i^z)$ is the spin operator at site i and the parameter λ accounts for the anisotropy interaction amongst spins: for $\lambda > 0$, spins tend to align along the internal Z axis (easy-axis regime); for $\lambda = 0$, one gets the isotropic case; for $-1 < \lambda < 0$, we have the easy-plane regime, while the $\lambda = -1$ case yields to the so-called XY model, which has been recently considered in curved surfaces²³. If we focus on a two-component spin, imposing $m_z \equiv 0$, so that $\vec{m}_{RPM} = (m_x, m_y)$, we get the planar rotator model (PRM).

In the continuum approach of spatial and spin variables, valid at sufficiently large wavelength and low temperature, the model given by (1) may be written as follows ($J \equiv J'/2$):

$$H = J \iint \sum_{i,j=1}^2 \sum_{a,b=1}^3 g^{ij} h_{ab} (1 + \delta_{a3} \lambda) \left(\frac{\partial m^a}{\partial \eta_i} \right) \left(\frac{\partial m^b}{\partial \eta_j} \right) \sqrt{|g|} d\eta_1 d\eta_2 \quad (2)$$

where the surface has curvilinear coordinates η_1 and η_2 , $\sqrt{|g|} = \sqrt{|\det[g_{ij}]|}$, g^{ij} and h_{ab} are the surface and spin space metrics, respectively (as usual, $g^{ij}g_{jk} = \delta_k^i$). Now, $\vec{m} = (m_x, m_y, m_z) \equiv (\sin \Theta \cos \Phi, \sin \Theta \sin \Phi, \cos \Theta)$ is the classical spin vector field valued on a unity sphere (internal space), so that $\Theta = \Theta(\eta_1, \eta_2)$ and $\Phi = \Phi(\eta_1, \eta_2)$. With this, the Cartesian parametrization for \vec{m} yields to $h_{ab} = \delta_{ab}$. The Hamiltonian (2) may be also viewed as the anisotropic non-linear σ model (NL σ M), which lies on an arbitrary two dimensional geometry.

III. DEVELOPMENT OF THE MODEL ON THE CONSIDERED SURFACES

Our interest is to study the above model on surfaces with negative and variable curvature. In this way, we are considering two curved surfaces with cylindrical-like shape, the catenoid and the hyperboloid. Here, we improve the results of Dandoloff *et al*²², for the catenoid and hyperboloid cases, with an analysis of the anisotropic Heisenberg model, in order to understand the energy properties of topological solitons and vortices in these geometries. Besides it, we compare the energy of these topological excitations with that obtained for the cylinder.

For our purposes, initially we will describe the mathematical properties and will apply the continuous anisotropic Heisenberg model on each surface, in order to obtain the Euler-Lagrange equations derived from the Hamiltonians obtained.

A. Catenoid

The first geometry to be considered is that of the catenoid, which is a nonplanar minimal surface, since it has the property that its mean curvature is everywhere zero. The catenoid is a surface that has the fascinating property that it can be deformed into a helicoid in such a way that every surface along the way is a minimal surface, which is locally isometric to the helicoid. Researches show that a soap film formed between two coaxial rings takes on the shape of a catenoid²⁴ and still, this geometry appears in membrane fissions and the characteristic of the neck shape is determined by the relationship between the neck radius and the monolayer thickness²⁵.

The catenoid can be parametrized by:

$$x = \rho \cosh\left(\frac{z}{\rho}\right) \cos \varphi, \quad y = \rho \cosh\left(\frac{z}{\rho}\right) \sin \varphi, \quad (3)$$

where $\varphi \in [0, 2\pi]$, $z \in (-\infty, \infty)$ and ρ is the radius of the circle in the $z = 0$ plane.

To describe our theoretical model in the geometry of the catenoid, we have assumed cylindrical symmetry to the spin coordinate system, that is, $\Theta \equiv \Theta(z)$ and $\Phi \equiv \Phi(\varphi)$. From Eq. (2), we have that $(\partial_\nu \Psi \equiv \frac{\partial \Psi}{\partial \nu})$:

$$H_{\text{cat}} = J \int_{-\pi}^{\pi} \int_{z_1}^{z_2} \left[\rho(1 + \lambda \sin^2 \Theta) (\partial_z \Theta)^2 + \frac{1}{\rho} \sin^2 \Theta (\partial_\varphi \Phi)^2 \right] dz d\varphi. \quad (4)$$

In this way, the Euler-Lagrange equations yield to:

$$2(1 + \lambda \sin^2 \Theta) \rho \partial_z (\rho \partial_z \Theta) = \sin 2\Theta [(\partial_\varphi \Phi)^2 - \lambda (\rho \partial_z \Theta)^2] \quad (5)$$

and

$$\partial_\varphi^2 \Phi = 0 \longrightarrow \Phi = \mathcal{Q}\varphi + \varphi_0 \quad (6)$$

where $\mathcal{Q} \in \mathbb{Z}$ and φ_0 are constant parameters that do not matter in the energy calculations. The Eq. (6) has the same form to the hyperboloid, in this way, we have omitted it in the following case.

B. Hyperboloid

The hyperboloid is a quadratic surface which may be one- or two-sheeted. The one-sheeted hyperboloid is a surface of revolution obtained by rotating a hyperbola about the perpendicular bisector to the line between the foci, that is, about the z axis, while the two-sheeted hyperboloid is a surface of revolution obtained by rotating a hyperbola about the line joining the foci.

When oriented along the z -axis, the one-sheeted circular hyperboloid with skirt radius ϱ has its parametrization given by:

$$x = \varrho \sqrt{1 + \eta^2} \cos \varphi, \quad y = \varrho \sqrt{1 + \eta^2} \sin \varphi \quad \text{and} \quad z = b\eta. \quad (7)$$

In spite of the hyperboloid to have a shape similar to the catenoid, the last one has mean curvature null everywhere, while the mean curvature of the hyperboloid is given by²⁶:

$$K_{\text{hyp}} = \frac{b^2[\varrho^2(\eta^2 - 1) + b^2(1 + \eta^2)]}{2\varrho[\varrho^2 + b^2(1 + \eta^2)]^{(3/2)}}. \quad (8)$$

So, unlike the catenoid, the hyperboloid is not a minimal surface. Besides it, there are substantial differences in their x, y coordinate values away from the plane $z = 0$, as well as in their geometrical properties.

For using the parametric equations (7), the anisotropic Heisenberg Hamiltonian (2) can be written as:

$$H_{\text{hyp}} = J \int_{-\pi}^{\pi} \int_{\eta_1}^{\eta_2} \left[\frac{1}{\chi'(\eta)} (1 + \lambda \sin^2 \Theta) (\partial_{\eta} \Theta)^2 + \chi'(\eta) \sin^2 \Theta (\partial_{\varphi} \Phi)^2 \right] d\eta d\varphi \quad (9)$$

where

$$\chi'(\eta) = \frac{\sqrt{b^2(1 + \eta^2) + \varrho^2 \eta^2}}{\varrho(1 + \eta^2)}. \quad (10)$$

The general parametrization given in Eq. (7) yields to hard integrals to be computed, so that, when necessary, these will be calculated numerically. A very useful kind of hyperboloid is given by the polar hyperbolic coordinate system (biharmonic coordinates), where $b = \varrho$. This particular coordinate system were recently used to develop the pseudospherical functions on an one-sheet hyperboloid²⁷, which are important if we consider cases where the solution of the Laplace Equation in problems with hyperbolic symmetry is necessary, e. g., it can be important to calculate the magnetostatic energy of hyperbolic magnets or the magnetic field inside a hyperbolic solenoid traversed by an electric current.

To the biharmonic coordinates, the characteristic length of the hyperboloid is given by:

$$\chi'_{b=\varrho}(\eta) \equiv \chi(\eta) = \frac{\sqrt{1 + 2\eta^2}}{1 + \eta^2}. \quad (11)$$

Finally, the Euler-Lagrange equation related to Eq. (9) is evaluated to give:

$$2(1 + \lambda \sin^2 \Theta) \frac{1}{\chi(\eta)} \partial_{\eta} \left(\frac{1}{\chi(\eta)} \partial_{\eta} \Theta \right) = \sin 2\Theta \left[(\partial_{\varphi} \Phi)^2 - \lambda \left(\frac{1}{\chi(\eta)} \partial_{\eta} \Theta \right)^2 \right]. \quad (12)$$

IV. DISCUSSION OF THE RESULTS

The results of the Euler-Lagrange equations (5) and (12) can be written in the below general form:

$$2(1 + \lambda \sin^2 \Theta) \partial_{\zeta}^2 \Theta = \sin 2\Theta [(\partial_{\varphi} \Phi)^2 - \lambda (\partial_{\zeta} \Theta)^2], \quad (13)$$

and the Hamiltonians (4) and (9) are rewritten as:

$$H_{\text{general}} = J \int_{-\pi}^{\pi} \int_{\zeta_1}^{\zeta_2} [(1 + \lambda \sin^2 \Theta) (\partial_{\zeta} \Theta)^2 + \sin^2 \Theta (\partial_{\varphi} \Phi)^2] d\zeta d\varphi, \quad (14)$$

where ζ is a parameter that depends of the characteristic length of each surface, that is:

$$\zeta_{\text{cat}} = \int \frac{1}{\rho} dz = \frac{z}{\rho} + \kappa_1 \quad (15)$$

and

$$\zeta_{\text{phyp}} = \int \chi(\eta) d\eta = \sqrt{2} \text{arcsinh}(\sqrt{2}\eta) + \frac{1}{4} \ln \left(\frac{1 + 3\eta^2 - 2\eta\sqrt{1 + 2\eta^2}}{1 + 3\eta^2 + 2\eta\sqrt{1 + 2\eta^2}} \right) + \kappa_2, \quad (16)$$

where κ_i ($i = 1, 2$) is an integration constant, ζ_{cat} and ζ_{phyp} are the parameters for the catenoid and polar hyperboloid, respectively. The integral associated to the ζ parameter for a general hyperboloid ($b \neq \varrho$) has not a simple solution and, when necessary, it will be calculated numerically.

As expected, the anisotropic Heisenberg model is described by nonlinear differential equations and suitable nontrivial solutions can be obtained provided that some conditions are imposed, so that special solutions, for the most general Eq. (13), will be obtained for solving it for two particular values of λ . Initially, we consider the isotropic case, where $\lambda = 0$ and after, we take $\lambda = -1$ to study the XY model, which simplest solution is a vortex. At this point, one can note that the equations above resemble in form those counterparts for the planar, cylindrical¹⁴, spherical¹³, pseudospherical¹² and toroidal¹⁰ surfaces. Indeed, whenever ζ is identified with $\int \frac{s}{\mathcal{R} + s \sin \theta}$, $\int \frac{1}{\mathcal{S} \sin \theta}$, or $\int \frac{1}{R\tau}$, while φ keeps its role as the azimuth-like angle, the equations above recover their toroidal, spherical or pseudospherical analogs. Above, \mathcal{R} and s are the rotating and axial radius of the torus, respectively, \mathcal{S} is the sphere radius and $R\tau$ accounts for the distance measured along pseudospherical geodesic, say, a hyperbole.

A. The $\lambda = 0$ case

When $\lambda = 0$, one get the isotropic Heisenberg model, which has been previosly studied on the surfaces considered²². In that work, skyrmion-like solutions were obtained, and half-skyrmions were found on the paraboloid surface. From now on, without lost of generality, we will take $\mathcal{Q} = 1$, what implies that the Eq. (13) is rewritten as:

$$2\partial_{\zeta}^2 \Theta = \sin 2\Theta, \quad (17)$$

that is the sine-Gordon equation, which solution can be given by²⁸:

$$\Theta(\zeta) = 2 \arctan(e^{\zeta}). \quad (18)$$

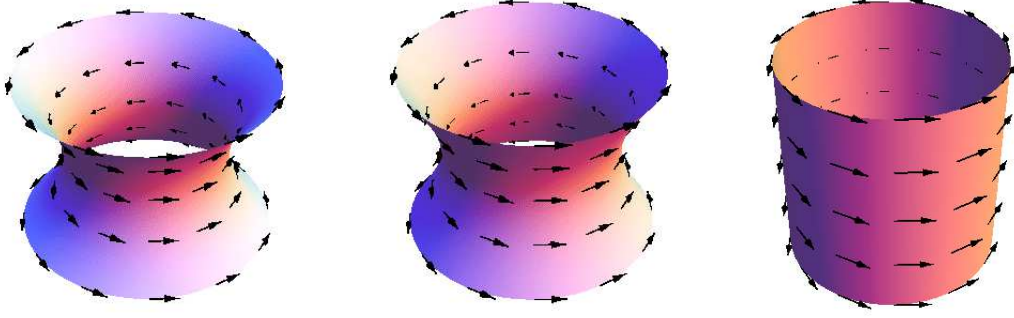


FIG. 1. [Color online] Vortex pattern with winding number $Q = 1$ on the surfaces of the catenoid, hyperboloid and cylinder. In these cases, the spins turn around the surface in a closed way. In spite of they have different shape, the characteristic length associated to the cylinder and catenoid are equal. Besides it, one can see that the shape of the catenoid and hyperboloid surfaces are similar, however, the mean curvature of the catenoid is null, while the mean curvature of the hyperboloid is nonzero. See discussion on the text.

From (14), the energy associated to the solution (18) is evaluated to give:

$$E_s = 2\pi J \int [(\partial_\zeta \Theta)^2 + \sin^2 \Theta] d\zeta = -\frac{8\pi J}{e^{2\zeta} + 1}. \quad (19)$$

Since the energy is lower than $8\pi J$, one can note that, if we consider a finite catenoid or hyperboloid, the Eq. (18) does not represent an integer π soliton. Indeed, it represents a half-soliton solution, which has not topological stability. However, when we have an infinity surface, one get an integer soliton, with energy $E_s = 8\pi J$, as predicted from the Bogomol'nyi inequality²⁹. An infinity catenoid (hyperboloid) can be obtained for taking $z_1(\eta_1) = -\infty$ and $z_2(\eta_2) = \infty$ in the Hamiltonians (4) and (9), respectively. Periodic soliton solutions also can be obtained to the surfaces considered here^{14,22} and the differences among the solitons in these and others geometries is associated with their characteristic lenght, which is closely related to the curvature of the surface²².

B. The $\lambda = -1$ case

In the model that we are leading, a vortex-like excitation can be obtained from the isotropic Heisenberg Hamiltonian, however, we have choosen to work with the XY model, where $\lambda = -1$, due to the fact that it inserts constraints in the solutions for Θ , which stay

confined in the xy -plane. In this case, the Eq. (13) is simplified to:

$$2 \cos^2 \Theta \partial_\zeta^2 \Theta = \sin 2\Theta [1 + (\partial_\zeta \Theta)^2], \quad (20)$$

for which the simplest solution is $\Theta = \pi/2$. From Eq. (6), we obtain a vortex with winding number $\mathcal{Q} = 1$, and the pattern, for the studied surfaces, can be viewed in the Fig. 1.

The vortex energy for each surface considered is determined from Eq. (14), that is evaluated to give:

$$E_{\text{vortex}} = 2\pi J \zeta \Big|_{\zeta_1}^{\zeta_2} \quad (21)$$

where ζ is given by the Eqs. (15) and (16), ζ_1 and ζ_2 are the lower and upper bounds of the integrals.

Now, we will proceed with the analysis about the vortex energy behavior in each surface separately. First, we will consider the catenoid case, where $\zeta_1 = -\frac{h}{\rho}$ and $\zeta_2 = \frac{h}{\rho}$. In this way, the Eq. 21 is evaluated to give:

$$E_{\text{vortex}}^{\text{cat}} = \frac{4\pi J h}{\rho}, \quad (22)$$

that is the same energy obtained if we consider a vortex on a cylinder surface with height $2h$ and radius ρ . This fact can be explained because these surfaces have the same characteristic length, $1/\rho$.

In the case of the hyperboloid, the characteristic length is given by $\chi'(\eta)$ and analytical calculations are possible only for the biharmonic coordinates, for taking the limits $\eta_1 = -h/\varrho$ and $\eta_2 = h/\varrho$. In this case, we have that:

$$E_{\text{vortex}}^{\text{hyp}} = 4\pi J \left[\sqrt{2} \operatorname{arcsinh} \left(\sqrt{2} \frac{h}{\varrho} \right) + \frac{1}{4} \ln \left(\frac{1 + 3 \left(\frac{h}{\varrho} \right)^2 - 2 \frac{h}{\varrho} \sqrt{1 + 2 \left(\frac{h}{\varrho} \right)^2}}{1 + 3 \left(\frac{h}{\varrho} \right)^2 + 2 \frac{h}{\varrho} \sqrt{1 + 2 \left(\frac{h}{\varrho} \right)^2}} \right) \right]. \quad (23)$$

Despite of the polar hyperbolic coordinates give us an analytical solution to the vortex energy, to compare the results obtained for this case with that of a catenoid and cylinder surfaces is not an immediate task, once the z coordinate varies with the radius ϱ (See Eq. (7)). In this way, it will be interesting to calculate numerically the vortex energy of the most general hyperboloid ($b \neq \varrho$) and analyse the vortex energy behavior with the radius ϱ . The numerical integration was done for using the Simpsons rule in a Fortran code, and the results can be viewed in Fig. 2.

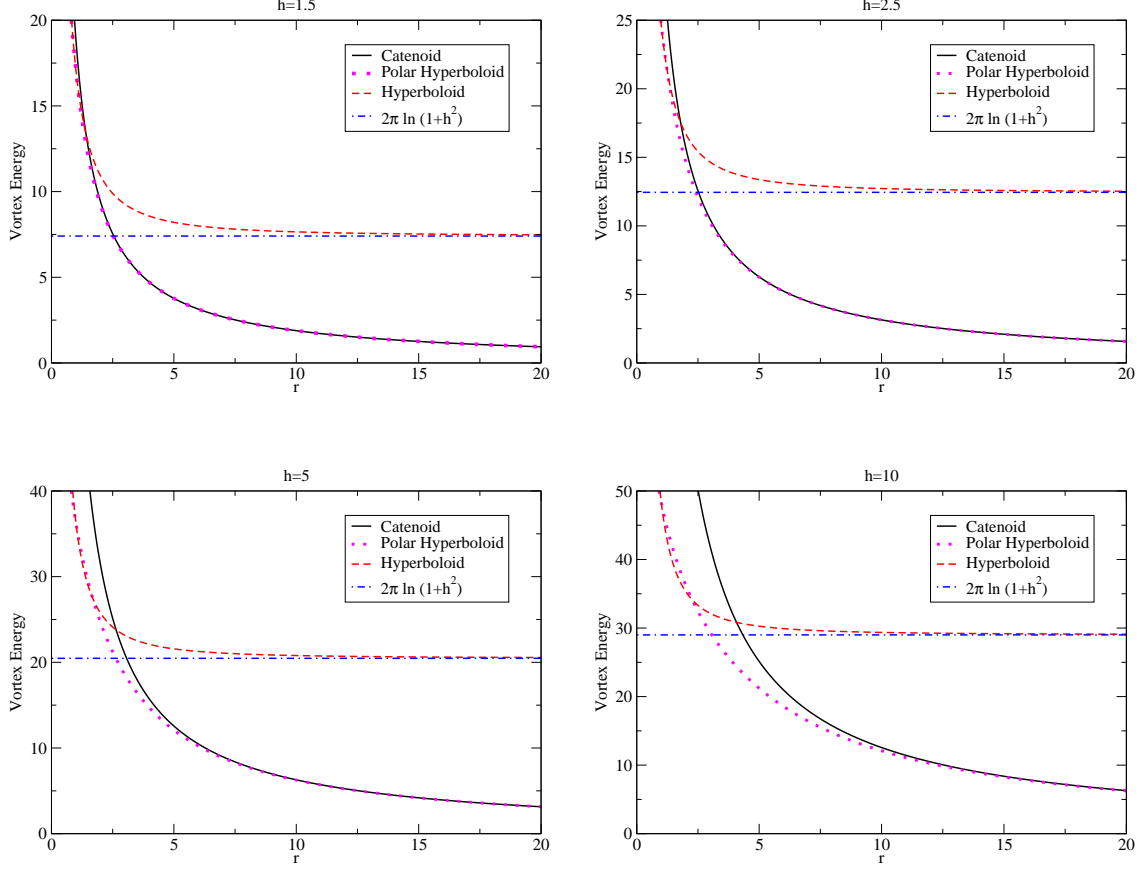


FIG. 2. [Color online] Vortex energy on the catenoid (black line) and the hyperboloid (red dashed line). Here, we have did $J = 1$, $b = 1$, ϱ is evaluated in the interval from 0.01 to 20. Four values of h are considered, $h = 1.5$ (top left), $h = 2.5$ (top right), $h = 5$ (bottom left) and $h = 10$ (bottom right). One can see that for small values of CR (central radius), the energy of a vortex on the hyperboloid has lower value than that of the vortex on a catenoid. However, for large values of CR, the vortex energy on a catenoid vanishes, while that of the hyperboloid tends to $2\pi \ln(1+h^2)$, which is the same value calculated to the energy of a vortex on a plane disc with external radius $1+h^2$ and a hole of radius 1 (represented in the figure by the dot-dashed blue line). The energy of a vortex on the polar hyperboloid (magenta dots) is always lower than that on a catenoid and, unlike the general hyperboloid ($b \neq \varrho$), it vanishes when $\varrho \rightarrow \infty$.

For continuing our analysis, it will be useful to define the central (CR) and upper radii (UR), that are the values of the radii of the surfaces in the plane $z = 0$ and $z = \pm h$, respectively. In this way, the cylinder, the catenoid and the hyperboloid have their UR

related by:

$$R_{\text{Upper}}^{\text{cyl}} = r, \quad R_{\text{Upper}}^{\text{cat}} = \rho \cosh\left(\frac{h}{\rho}\right) \quad \text{and} \quad R_{\text{Upper}}^{\text{hyp}} = \varrho \sqrt{1 + h^2}, \quad (24)$$

where r , ρ and ϱ are the CR of the cylinder, catenoid and hyperboloid ($b = 1$), respectively. When the CR of the three surfaces are equal, one can note, from Eq. (22), that the energy obtained to the catenoid is the same to that obtained for a vortex on the surface of the cylinder with height $2h$ and radius ρ . This is an interesting result, since the area of the catenoid is greater than that of the cylinder. This fact can be explained because these surfaces have the same characteristic length $1/\rho$. Besides it, from the analysis of the Fig. 1, one can note that, in the $z = 0$ plane, the neighbor spins on the catenoid must have the angle equal to that of the spins on the cylinder, however, when $z \neq 0$, the neighbor spins that turning around the catenoid surface have a lower deviation one to another, when compared with that of the cylinder, compensating the largest area, and diminishing the exchange energy (given by the Heisenberg model) in this plane.

The general hyperboloid case ($b \neq \varrho$) will be treated numerically, and the obtained results can be viewed in the Fig. 2, where we have did $b = 1$. One can note that, for small values of ϱ , the vortex on a hyperboloid has lower energy than that of a catenoid, however, when it increases, this behavior changes and the energy of a vortex on the hyperboloid is greater than that on the catenoid. This fact can be explained from the differences of properties of the two geometries when $r, \rho, \varrho \rightarrow \infty$ and the height h is maintained constant. While the catenoid has its UR related with the height by $\cosh(h/\rho)$, the hyperboloid grow with $\sqrt{1 + h^2}$, what implies that if $r \gg 1$, $R_{\text{Upper}}^{\text{cat}} \rightarrow R_{\text{Upper}}^{\text{cyl}}$ and $R_{\text{Upper}}^{\text{hyp}} \rightarrow \infty$. Indeed, for large CR, the catenoid surface looks like a cylinder, while the hyperboloid has the topology and geometry of a plane with a hole. In this way, the energy of a hyperboloid tends asymptotically to a value different from zero, e. g., $E_{\text{vortex}}^{\text{hyp}} \rightarrow 2\pi \ln(1 + h^2)$ when $\varrho \rightarrow \infty$. This is the second time that an hyperbolic surface presents nonzero energy when the characteristic radius of the surface tends to infinity¹². It is important to note that, unlike the catenoid case, the characteristic length of the hyperboloid tends not to zero when $\varrho \rightarrow \infty$, that is to say:

$$\chi'(\eta)_{\varrho \rightarrow 0} = \frac{\eta}{1 + \eta^2} \Rightarrow \zeta_{\text{hyp}}^{\varrho \rightarrow \infty} = \ln(1 + \eta^2). \quad (25)$$

From the analysis of the Fig. 2, one can see that the asymptotic value for the vortex energy on a hyperboloid is that of a plane disc with a hole with external radius $1 + h^2$ and internal

radius 1. Finally, when we increase the value of h , it is obtained that the value of ϱ of the transition point in which the vortex energy on the hyperboloid and on the catenoid intersect themselves increases from $\varrho \approx 2$ for $h = 1.5$ to $\varrho \approx 4$ for $h = 10$. The cases $b \neq 1$ do not have qualitative changes on the vortex energy behavior. In this case, the curve that characterizes the vortex energy is moved upwardly, however, as well as the $b = 1$ case, it tends to $2\pi \ln(1 + h^2)$, once the b value does not affect the ζ_{hyp} parameter when $\varrho \rightarrow \infty$, see Eq. 10).

Another interesting result appears when we analyse the polar hyperboloid case. Now, the vortex energy is always lower than that of the catenoid and as expected, for small CR ($\varrho \approx 1$), the energy is the approximately that obtained for the general hyperboloid and $E_{\text{phyp}} \rightarrow 0$ when $\varrho \rightarrow \infty$ (See Fig. 2). This can be explained because in this limit, the polar hyperboloid looks like a catenoid and has characteristic length given by:

$$\chi'(\eta)_{\varrho \rightarrow \infty} = 1 \Rightarrow \zeta_{\text{phyp}}^{\varrho \rightarrow \infty} = z/\rho = \zeta_{\text{cat}}. \quad (26)$$

The fact that the lowest value found for the vortex energy occurs on the polar hyperboloid indicates that, at first sight, among the surfaces considered here, this shape must support a vortex-like magnetization with more stability than the other ones, however, we must calculate the magnetostatic energy for other possible magnetization states and consider the volume of the magnet to ensure this affirmation.

If we consider the case where the UR of the three surfaces are equal, one can note immediately that the catenoid has lower energy than that of the cylinder, since the vortex energy for both surfaces is inversely proportional to the CR. However, there are not qualitative changes when we think in the hyperboloid case. Here, as well as the previous analysis, the energy of the three surfaces diminishes with the increasing of the UR, tending to zero when $r \rightarrow \infty$ (cylinder, catenoid and polar hyperboloid).

In conclusion, we can note that the energy of the vortex in the considered surfaces has a minimum value when the shape of the surface has a shape between the cylindrical and the catenoidal ones. In this way, if the CR are equal, and we begin to deform an elastic material with cylindrical shape with a vortex-like excitation till it forms a catenoid, its energy decreases, having a minimum on the polar hyperboloid shape, and after, increases again. In this way, an important task would be to find the geometry that gives the minimum value for the vortex energy for adding in this analysis surfaces with positive curvature.

It is important reinforce that the fact of the polar hyperboloid presents the lowest vortex energy does not ensure that nanomagnets with this geometry supports vortex magnetization configuration with more stability than cylindrical shell nanorings, once for applications in nanomagnetism, we must consider the volume of the nanoparticle and take account the magnetostatic energy to calculate the magnetic energy associated to other magnetization configurations.

V. CONCLUSIONS AND PROSPECTS

We have applied the anisotropic Heisenberg model to study topological spin excitations on the surfaces of the catenoid and hyperboloid, that have negative and variable Gaussian curvature. When we consider the isotropic case ($\lambda = 0$), we got soliton-like solutions and the energy associated to these excitations obey the Bogomolny'i inequality. For $\lambda = -1$, one obtain the XY model, which simplest solution is a vortex with winding number $\mathcal{Q} = 1$. The energy associated to these vortices, for each surface, was compared with that presented for a vortex on the cylinder. It is observed that for small CR, the general hyperboloid ($b \neq \varrho$) presents a vortex energy lower than that for the cylinder and catenoid, however, with its increasing, unlike the catenoid case, the vortex energy on a hyperboloid does not vanishes. The shape that presents the lowest value for the vortex energy is the polar hyperboloid, what can indicate that, for magnetic systems, this shape would be the best for support the vortex magnetization configuration.

This work is important if we think in magnetoelastic membrane manipulations, what could be done by the application of an external magnetic field on a magnetoelastic surface¹⁹ or from the concept of magnetoelastic metamaterial, which can response to an external field with a deformation, what is achieved by providing a mechanical degree of freedom so that the electromagnetic interaction in the metamaterial lattice is coupled to elastic interaction³⁰. In this way, the results obtained here can be interesting on this subject, once vortices could be used to deform the shape of magnetoelastic surfaces to obtain a particular shape. It must be an important task to study the vortex energy for surfaces with positive mean curvature and determinate what is the surface that has the minimum value for the vortex energy.

The results obtained here also are important if we think in miniaturization of magnetic elements, because it can help to understand the influence of the curvature in magnetic

properties of nanostructures as well as the vortex stability in ferromagnetic nanoparticles. Indeed, nanomagnets with vortex as magnetization ground states has been considered to compose data storage elements and nanoparticles for cancer therapy. So, at first sight, this work can indicate that to insert curvature in cylindrical nanomagnets could improve the vortex stability in these structures.

Acknowledgements

We thank to the brazilian agency CNPq (project number 562867/2010-4), for financial support. We also are grateful to J. S. Santos, W. A. Moura-Melo and A. R. Pereira for fruitful discussions.

* vagson.santos@ufv.br

- ¹ J. M. Kosterlitz, and D. J. Thouless, J. Phys. C: Solid State Phys. **6**, 1181 (1973).
- ² W. T. M. Irvine, V. Vitelli, and P. M. Chaikin, Nature **468**, 947 (2010).
- ³ S.-B. Choe, Y. Acremann, A. Scholl, A. Bauer, A. Doran, J. Stohr, and H. A. Padmore, Science **304**, 420 (2004); A. Wachowiak, J. Wiebe, M. Bode, O. Pietzsch, M. Morgenstern, and R. Wiesendanger, Science **298**, 577 (2002); V. Novosad, K. Yu. Guslienko, H. Shima, Y. Otani, K. Fukamichi, N. Kikuchi, O. Kitakami, and Y. Shimada, IEEE Trans. on Magnetics, **37**, (2001).
- ⁴ X. Z. Yu, Y. Onose, N. Kanazawa, J. H. Park, J. H. Han, Y. Matsui, N. Nagaosa, and Y. Tokura, Nature **465**, 901 (2010); K.-S. Lee, M.-W. Yoo, Y.-S. Choi, and S.-K. Kim, Phys. Rev. Lett. **106**, 147201 (2011).
- ⁵ R. P. Cowburn, D. K. Koltsov, A. O. Adeyeye, M. E. Welland, and D. M. Tricker, Phys. Rev. Lett. **83**, 1042 (1999).
- ⁶ A. Vansteenkiste, M. Weigand, M. Curcic, H. Stoll, G. Schütz, and B Van Waeyenberge, New Journal of Physics **11**, 063006 (2009).
- ⁷ V. Vitelli, and A. M. Turner, Phys. Rev. Lett. **93**, 215301 (2004).
- ⁸ V. L. Carvalho-Santos, W. A. Moura-Melo, and A. R. Pereira, J. Appl. Phys. **108**, 094310 (2010).
- ⁹ F. A. Apolonio, W. A. Moura-Melo, F. P. Crisafuli, A. R. Pereira, and R. L. Silva, J. Appl. Phys. **106**, 084320 (2009).

- ¹⁰ V. L. Carvalho-Santos, A. R. Moura, W. A. Moura Melo, and A. R. Pereira, Phys. Rev. **B 77**, 134450 (2008).
- ¹¹ J. Benoit, and R. Dandoloff, Phys. Lett. **A 248**, 439 (1998); A. Saxena, R. Dandoloff, and T. Lookman, Physica **A 261**, 13 (1998);
- ¹² L. R. A. Belo, N. M. Oliveira-Neto, W. A. Moura-Melo, A. R. Pereira, and E. Ercolessi, Phys. Lett. **A 365**, 463 (2007).
- ¹³ G. S. Milagre, and W. A. Moura-Melo, Phys. Lett. **A 368**, 155 (2007).
- ¹⁴ S. Villain-Guillot, R. Dandoloff, A. Saxena, and A. R. Bishop, Phys. Rev. **B 52**, 6712 (1995); L. A. N. de Paula, Bras. Journ. of Phys. **39**, 711 (2009).
- ¹⁵ W. A. Freitas, W. A. Moura-Melo, and A. R. Pereira, Phys. Lett. **A 336**, 412 (2005); W. A. Moura-Melo, A. R. Pereira, L. A. S. Mól, and A. S. T. Pires, Phys. Lett. **A 360**, 472 (2007).
- ¹⁶ A. Saxena, and R. Dandoloff, Phys. Rev. **B 66**, 104414 (2002).
- ¹⁷ V. P. Kravchuk, D. D. Sheka, R. Streubel, D. Makarov, O. G. Schmidt, and Y. Gaididei, Phys. Rev. **B 85**, 144433 (2012).
- ¹⁸ J. Gravesen, and M. Willatzen, Phys. Rev. **A 72**, 032108 (2005); V. Atanasov, and R. Dandoloff, Phys. Lett. **A 371**, 118 (2007); V. Atanasov, and R. Dandoloff, Phys. Lett. **A 372**, 6141 (2008); Bjørn Jensen, Phys. Rev. **A 80**, 022101 (2009); V. Atanasov, R. Dandoloff, and A. Saxena, Phys. Rev. **B 79**, 033404 (2009).
- ¹⁹ A. Saxena, and R. Dandoloff, Phys. Rev. **B 58**, R563 (1998).
- ²⁰ J.-G. Dai, Y. Zheng, and G. A. Prinz, J. Appl. Phys. **87**, 6668 (2000); G. A. Prinz, J. Magn. Mag. Mat. **200**, 57 (1999); S. H. Sun, C. B. Murray, D. Weller, L. Folks, and A. Moser, Science **287**, 1989 (2000); G. A. Prinz, Science **282**, 1660 (1998).
- ²¹ D.-H. Kim, E. Rozhkova, I. Ulasov, S. Bader, T. Rajh, M. Lesniak, and V. Novosad, Nature Matter., DOI: 10.1038/NMAT2591 (2009); E.A. Rozhkova, V. Novosad, D.-H. Kim, J. Pearson, R. Divan, T. Rajh, and S. D. Bader, J. Appl. Phys. **105**, 07B306 (2009); E.A. Rozhkova, I. Ulasov, B. Lai, N. M. Dimitrijevic, M. S. Lesniak, and T. Rajh, Nano Lett. **9**, 3337 (2009).
- ²² R. Dandoloff, and A. Saxena, J. Phys. A: Math. Theor. **44**, 045203 (2011).
- ²³ R. Dandoloff, and A. Saxena, Phys. Lett. **A 358**, 421 (2006); X. Peng, S. Wu, J. Li, D. Suter, and J. Du, Phys. Rev. Lett. **105**, 240405 (2010); Y. Komura, and Y. Okabe, J. Phys. A: Math. Theor.: **44**, 015002 (2011).
- ²⁴ T. R. Powers, G. Huber, and R. E. Goldstein, Phys. Rev. **E 65**, 041901 (2002).

- ²⁵ Y. Kozlovsky, and M. M. Kozlov, Biophys. J. **85**, 85 (2003).
- ²⁶ E. W. Weisstein, "*Hyperboloid*." From MathWorld - A Wolfram Web Resource.
<http://mathworld.wolfram.com/Hyperboloid.html>
- ²⁷ K. Kowalski, J. Rembieliński, and A. Szcześniak, J. Phys. A: Math. Theor.: **44**, 085302 (2011).
- ²⁸ R. Rajaraman, *Solitons and Instantons: An Introduction to Quantum Field Theory* (North-Holland, Amsterdam, 1984).
- ²⁹ E. B. Bogomolnyi, Sov. J. Nucl. Phys. **26**, (1976) 449.
- ³⁰ M. Lapine, I. V. Shadrivov, D. A. Powell, and Y. S. Kivshar, Nature Materials **11**, (2012) 30.